Journal of Membrane Science and Research 7 (2021) 209-223

Journal of Membrane Science & Research

journal homepage: www.msrjournal.com

Research Paper

Experimental, Modeling and AspenPlus Simulation of Different Configurations of Membrane Separation Systems for Highly Loaded CO_2 Selective Pebax 1657-ZIF-8 Membrane

Abolfazl Jomekian [1,*], Reza Mosayebi Behbahani [2]

[1] *Esfarayen University of Technology, Esfarayen, North Khorasan, Iran*
[2] *Chemical Engineering Department, Ahvaz Faculty of Petroleum Engineering, Petroleum University of Technology (PUT), Ahvaz, Iran*

Article info

Received 2020-09-22
Revised 2020-11-22
Accepted 2020-11-26
Available online 2020-11-26

Keywords

CO_2/CH_4 separation
ZIF-8
Pebax 1657
Ionic liquid
Aspen Plus

Graphical abstract

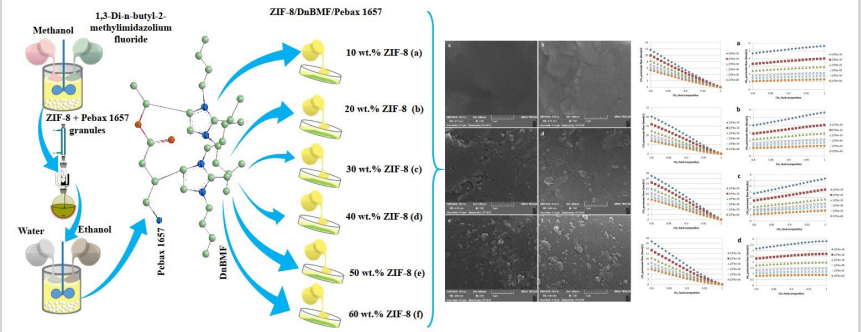

Highlights

- High content of ZIF-8 were introduced into the matrix of functionalized Pebax 1657.
- ^{13}CNMR analysis revealed that C-C bond formed at ZIF-8 particle-polymer interface.
- Gas permeation test showed effectiveness of IL-modified ZIF-8/Pebax MMMs.
- Microsoft Excel was linked to Aspen Plus for modeling and simulation.
- Simulation results suggest that recycle of products was effective in separation boost.

Abstract

ZIF-8 powder was synthesized and added with concentrations from 10 to 60 wt.% to the Pebax 1657 matrix modified with Di-butyl-methylimidazolium fluoride (DBMF) ionic liquid. SEM, XRD and ^{13}C-NMR analysis were applied for the characterization of particles and mixed matrix membranes (MMMs). The results of ^{13}C-NMR analysis suggested that there are possible new carbon-carbon bonds at particle-polymer interface. The CO_2/CH_4 mixed gas test results showed that the utilization of high concentrations of ZIF-8 in Pebax 1657 matrix was effective. MMMs containing 60 wt.% and 30 wt.% of ZIF-8 showed the highest (24.4) and lowest (12) CO_2/CH_4 selectivity among the all synthesized MMM and pure polymeric samples, respectively. The results of the Microsoft Excel/Aspen Plus modeling and simulation showed that the increase in membrane area, number of membrane modules and the pressure difference across membranes led to performance advantages for the single-step with permeate recycling (SiSRP) and double step with retentate recycling (DoSRR) configurations of separation systems. The highest CH_4 recovery was observed for the double-step with permeate recycling (DoSPR) configurations when the feed was nearly pure CH_4. The temperature rise showed a notable increasing effect on permeates flow rates of both gases leading to the deterioration of the separation effectiveness for all configurations. The analysis of membrane thickness on gas permeation showed that the synthesis of thinner membranes leads to better separation performance utilizing permeant or/and retentate recycle lead to more purified products.

1. Introduction

CO_2 is the source of many global problems, such as the reduction of the heat value of natural gas, pipeline rusting, and pressure drop and hydrate formation in the natural gas industry [1-3]. Although the traditional CO_2 separation operations, such as absorption by amines [4] or cryogenic operations [5], showed a great effectiveness in CO_2 capture from natural gas, these methods consume a huge amount of energy, and these days processes with a high level of fuel consumption are not favored by industry. Membranes, as one of the most interesting methods of CO_2 separation, have emerged because membrane operations are economically attractive and they are easy to use and apply [6]. Hence, the number of researches on the different types of membrane has increased dramatically, particularly for CO_2 separation applications. Multilayer MMMs with a combined selective layer and a porous substrate, have been proven to be effective in CO_2 capture [7,8]. The material selection, design, and concentration for the preparation of the selective layer are very important in MMMs synthesis. Pebax 1657 or Poly(ether-block-amide) 1657 copolymer, which is fabricated by a combination of PEO and PA6 segments, showed effectiveness in CO_2 capture and it has been used by many groups as the selective layer main synthesis

* Corresponding author:E-mail address: a_jomekian@esfarayen.ac.ir (A. Jomekian)

DOI: 10.22079/JMSR.2020.136920.1411

material [7,9]. Different types of modification of these membranes were applied to several kinds of copolymer and Pebax 1657 membranes in recent years [7,10-13]. Incorporation of ionic liquid in functionalization of polymeric materials for the improvement of the separation effectiveness and compatibility improvement at the polymer-particle interface can be named as methods that have been examined by several groups [9,11,13-15]. Fam and his group [7] published the introduction of [emim][BF4] in the modification of Pebax 1657 for improvement of separation of CO_2. Bernardo and his colleagues [16] successfully fabricated and tested a Pebax membrane applying an ionic liquid composed of imidazole groups to boost the ability of the membrane's CO_2 capture. Rabiee et al. [17] entered an ionic liquid into Pebax synthesis medium for the elevation of separation performance of CO_2 from H_2. The works that have been performed on the application of ILs based on imidazole groups in the Pebax solution indicated interesting performance in CO_2 capture. On the other hand, in recent years number of studies on modification of MOFs and its subgroups on different applications such as gas adsorption notably elevated [18-20]. ZIF-8, as the most attractive member of the ZIF family, which is a subgroup of MOFs, has been utilized in MMMs for sorption of CO_2 because of its outstanding CO_2-philic property. According to previous studies [21-25], high concentrations of Zeolitic Imidazolate Frameworks-8 (ZIFs) in the matrix of polymer resulted in significant improvement in separation ability of membranes while the mechanical instability of MMMs limited further rise in concentration of filler because of the loss of required flexibility for integrity of selective layer. To tackle this problem, one interesting idea which was examined in some previous works [22,26-29], is the utilization of imidazolium based ILs for enhancement of interaction between polymer and ZIF particle. The imidazole group of ILs was observed to interact strongly with imidazole group of ZIF particles [9,26-29]. Therefore in this work, Di-butyl-methylimidazolium Fluoride (DBMF) an effective and rarely studied type of imidazole based ionic liquid with proven high affinity for CO_2 was synthesized and introduced in the preparation process of ZIF-8 for improvement in CO_2/CH_4 separation properties of resulted MMMs.

There are several different configurations for operating membrane separation systems such as single-step, single-step with the recycling of permeate, the double-step with the recycling of permeate, the double-step with the recycling of retentate, etc. There are well-known commercially available pieces of software such as Aspen Plus and Aspen HYSYS for chemical process simulations. However, the model library in none of these two pieces of software involves any membrane build-in model. It can be placed, designed and programmed mathematically applying FORTRAN or Microsoft Excel. Rautenbach et al. [30] presented a membrane system configuration in Aspen Plus for three different separation processes neglecting the pressure drop. Davis [31] ignored the effect of a significant pressure drop in Aspen HYSYS and created a hollow fiber model for membrane without custom programming. In another work, Chowdhury et al, [32] implemented Pan model [33] into Aspen Plus using a numerical solution approach for parallel membrane steams configurations. A successful single dimension model in Aspen HYSYS for a facilitated transport membrane separation case of CO_2 capture was presented by Hussain and Hagg [34]. Despite the remarkable efforts in the mentioned works, the lack of a comprehensive and simple approach that includes configurations of single and several step systems modeled based on permeation data from as-synthesized high-performance MMMs is felt. Therefore, in this work, initially Pebax 1657 membranes with elevated concentrations of ZIF-8 was fabricated by incorporation of DBMF ionic liquid to enhance the particle-polymer compatibility, then the membrane was characterized using SEM, XRD and ^{13}C-NMR spectroscopy. The permeation data was gathered from binary gas permeation experiments and the results have been used as input in membrane modeling for the separation performance comparison of different membrane systems configurations.

2. Materials and Methods

2.1. Materials

Pebax has been procured from Arkema Incorporation. Nonwoven polyester was supplied by NIPC inc., Sodium Hydroxide (NaOH, 99.5%) and Acetonitrile (ACN, 99.5%) were supplied from Guangzhou Sinosource Inc. 1-fluorobutane was bought from Atomax Inc. ($Zn(NO_3)_2.6H_2O$, 99.5%), 2-methyl Imidazole (MeIM, 99.5%), (MeOH, 99.98 %), (Dimethylformamide (DMF, 99.98%), Ethanol (EtOH, 99.98%), Distilled Water and (n-hexane, 99.98%) were supplied by Merck.

2.2. ZIF-8 powder synthesis

Several grams of $Zn(NO_3)_2.6(H_2O)$ and MeIM granules were first put at 70 °C for 2 h. According to our previous experience [35] to prepare the smallest ZIF-8 samples, $MeIM/Zn(NO_3)_2$. $6(H_2O)$ with the ratio of 32 was used for the preparation of ZIF-8, using 1 g of $Zn(NO_3)_2$. $6(H_2O)$ and 13.87 g of MeIM. Each precursor was stirred in 100 ml of DMF solvent for 30 min. Then both clear solutions merged and stirring continued for an additional 2 h. The procured milky suspension was centrifuged for 20 min and finally washed with methanol. The final resulted powder was distributed on a dish at 30 °C for 24 hours to dry.

2.3. Synthesis of Di-butyl-methylimidazolium fluoride ionic liquid

First, 1.5 g of NaOH and 2.6 g of 2-methylimidazole were poured into 25 ml of ACN and dissolved by gentle stirring for 1 h, then1-fluorobutane was poured slowly into ACN solution. An additional 60 min of stirring resulted in butyl-methylimidazole formation. 1-fluorobutane was poured into the as-prepared butyl-methylimidazole solution and the obtained solution was continued to stir for 6 h at 100 °C. Di-butyl-methylimidazolium fluoride was removed using batch distillation at the temperature of 70 °C.

2.4. Preparation of supported IL modified membranes

2 g of Pebax has been suspended in a mixture made of 24 ml Di-butyl-methylimidazolium fluoride and 24 ml methanol. The obtained sample has been stirred at 75 °C for 10 h, and then the Pebax granules modified with IL were collected and washed twice with fresh methanol. These prepared granules stirred in 60 ml of ethanol and 30 ml of water for 24 h at 70 °C. Different quantities of as-prepared ZIF-8 powder was wetted in 10 ml of ethanol before adding to the Pebax 1657 solution to avoid possible agglomeration of particles. This suspension was then poured into the Pebax 1657 solution followed by three cycles of stirring and ultrasonic operations bath (each 10 min).

The resulted solution was aged for 3 h for bubble removal. Then the nonwoven polyester support was fixed on top of flat glass by tapes. The casting of the modified Pebax 1657 solution was performed using a casting knife (ZEHNTNER, ZUA 2000). The resulted membrane film was put at 30 °C for 24 h for evaporation of the solvent. The ZIF-8 content and code name of samples are shown in Table 1. It has to be noted that a pure ZIF-8 sample, an unmodified ZIF-8-Pebax 1657 membrane, and a pristine membrane were synthesized for comparison purposes.

Table 1
Code names of synthesized membrane samples with their ZIF-8 content (Pbx is an abbreviation for Pebax).

Code names of membranes	ZIF-8 content in MMM selective layer (wt. %)	ZIF-8 quantity in synthesis solution (g)
Z/Pbx-10	10%	0.22
Z/Pbx-20	20%	0.5
Z/Pbx-30	30%	0.86
Z/Pbx-40	40%	1.33
Z/Pbx-50	50%	2
Z/Pbx-60	60%	3
ZIF-8	100%	4
***Pbx**	0	0
****UZ/Pbx-10**	10%	0.22

* This sample is synthesized similar to other IL modified samples excluding ZIF-8 incorporation.
** This sample is synthesized similar to (Z/Pbx-10) sample excluding IL incorporation.

2.5. CO_2 and CH_4 permeance measurements

A pre-designed and manufactured permeation set-up was used for the immurements of permeances of CO_2 and CH_4. This set-up operated with variable-volume and constant pressure settings using two hand-made flat membrane modules (see Supplementary file, Fig. S1). The binary mixed-gas tests were performed at 20 bar feed pressure. Using the permeation setup, 10-90 vol.% of CO_2-CH_4 binary gas mixtures have been made to test the membranes.

The gas permeances have been calculated by the following formula [12,36]:

$$P_i = \frac{y_i Q}{A(p_f x_i - p_p y_i)} \quad (1)$$

where P_i is permeance of gas i, x_i and y_i are in respective feed and permeate side mole fractions of gas i, A is permeable membrane area (cm^2), and p_p and p_f are in respective, permeate side and feed side pressures (cmHg).

The division of permeance of gas (A) to gas (B) is defined as selectivity $\alpha_{A/B}$ by the following formula:

$$\alpha_{A/B} = \frac{P_A}{P_B} \quad (2)$$

A TCD detector installed in a GC (ACME 6100, Korea) was used for the detection of gases exiting GC columns. The data from the TCD detector was used for the exact determination of the composition of permeate flow.

1.6. Characterization

To check the ZIF-8 formation and purity of its crystalline phase, X-ray diffraction analysis (Shimadzu, XRD-6100) was applied. The diffractometer was set to operate with radiation (30 mA and 35 kV) and with a scanning range of $1° \leq 2\theta \leq 60°$. A scanning electron microscope (SEM) (TESCAN-MIRA3) was utilized for the investigation of the structure of the membrane. To scrutinize the possible formation of carbon-carbon single bonds sue to the IL modification in MMMs, (^{13}C NMR) spectroscopy was exploited. ^{13}C NMR patterns of samples were recorded from a spectrometer (400 MSL NMR, Bruker). The solvent that was selected for ^{13}C NMR spectroscopy was ethanol-d_6 and the reference material for chemical shifts was tetramethylsilane.

2. Modeling and Simulations

The well-known and widely accepted solution-diffusion mechanism was selected as the base of modeling in this work. The rearrangement and modification of eq. (1) yields the governing equations for the calculation of gas flux:

$$J_{CO_2} = \frac{yQ}{A} = P_A[p_f x - p_p y] \quad (3)$$

$$J_{CH_4} = \frac{(1-y)Q}{A} = P_B[p_f(1-x) - p_p(1-y)] \quad (4)$$

Dividing two above equations gives:

$$\frac{y}{1-y} = \alpha \frac{p_f x - p_p y}{p_f(1-x) - p_p(1-y)} \quad (5)$$

where y and x are in respective the composition of more permeable gas (CO_2) in the permeate and feed streams, α is the CO_2/CH_4 selectivity of the membrane.

Rearranging Eq. (5) in the form of the second-order linear algebraic equation gives:

$$\left(\frac{p_p}{p_f} - \alpha\left(p_p - p_f\right)\right)y^2 + \left(1 - x + \alpha x - \frac{p_p}{p_f} + \alpha\left(p_p - p_f\right)\right)y - \alpha x = 0 \quad (6)$$

Solving this equation gives y and therefore the permeating flux through the membrane (J). Since the modules of membranes have limited effective area for permeation, there must be numerous membrane modules in the purification process:

$$J_{total} = nJ_{single} \quad (7)$$

The permeabilities and therefore permeances of CO_2 and CH_4 through MMMs depend on temperature based on the Arrhenius-type equation:

$$P = P_0 \exp\left(-\frac{E_p}{RT}\right) \quad (8)$$

In which P_0 is a constant determined from exponential data fitting with experimental data, EP is the activation every of permeation of gases (kJ/mol), R is (0.008314 kJ/(mol.K)) and finally, the temperature (K) is shown by T.

An Aspen Plus ver. 10 simulation environment was utilized to simulate the single-step and double step membrane configurations with the equation of state such as Peng-Robinson as the base method. Aspen Plus model library does not include a membrane separation system, hence a costume membrane model was designed and programmed using "User Model, User 2 subroutine" in Aspen plus model library. This model can be linked to a Microsoft Excel file as a source environment for the definition of variables and calculation of parameters. The membrane model relationships along with the experimental permeances and selectivities of different membranes were introduced in Microsoft Excel in AspenONE-Microsoft Excel interface. Each membrane block has its own Microsoft Excel file which is uniquely designed and programmed. The input data has been defined and their values have been entered in Aspen plus membrane module environment. This data is transferred to Microsoft Excel as input, then the calculations have been programmed and performed in an Excel environment finally the results have been transferred back to Aspen plus environment to be presented to the user as the result of the simulation. The defined variables in the Aspen Plus membrane model are presented in Table S1 (refer to the Supplementary materials).

The membrane process system design is mainly based on parameters of each membrane modules and the configuration of them. If high purity is not exigent, a single-stage membrane separation system configuration results in satisfying recovery. However, for high purity separation demands, it is necessary to utilize multiple-stage membrane separation system which can use permeate or retentate as a recycle stream. The system design with several stages is highly complicated since it is not possible to account for all membrane system shapes. Two different points of view might be regarded to optimize and design of a flowsheet and its related operating states. One is to synthesize a membrane system that includes all practical configurations, apply nonlinear programming (NLP) to the systems included, and develop a suitable solution strategy. This approach suffers from a major disadvantage which is except for the cases that specific routes for optimization are used, the global optimization parameters cannot be easily found for unconventional models unless special procedures are applied for global optimization. Another method is to select a limited number of designs and try to optimize the selected designs for the best separation performance. In this work, we decided to apply the second approach to design the membrane system. Hence, four different configurations of membrane systems have been simulated in Aspen Plus: The single-step (SiS), the single-step with the recycling of permeate (SiSRP), the double-step with the recycling of permeate (DoSRP), and double step with the recycling of retentate (DoSRR). The process flow diagrams of these simulations are presented in Fig 1 a-d. The sensitivity analysis in Aspen plus has been applied to investigate the effect of defined variables on the permeate flux of each membrane system configuration.

3. Results and discussions

3.1. Results and Discussions of Experiments

3.1.1. SEM

The cross-sectional SEM images of IL-modified MMMs are presented in Fig. 2a-f. In all SEM images, a relatively thin selective layer is observable on top of a porous thick sub-layer of non-woven polyester which demonstrates the integrity of casting of ZIF-8/Pebax 1657 solution on support. The porosity of the nonwoven polyester substrate is observable in all subfigures. This highly porous substrate appears to show negligible resistance against gas flux. The relatively thick substrate with a thickness over 100 µm can provide enough mechanical strength for the selective layer especially for the permeation experiments with high feed gas pressure. In all of the MMM samples, the substrate layer is notably rough. Hence the SEM micrograph from the surface of samples is also needed to conclude the integrity of the selective layer.

The SEM micrographs from the surface of all improved membranes are provided in Fig. 3 a-f.

The ZIF-8 concentration elevation in the synthesis solution causes the roughness of the surfaces of the membranes to increase significantly. This is because all of the MMMs in the study have been synthesized with unconventionally high concentrations of ZIF-8, hence, the partial aggregation of particles at the surface of the membrane is unavoidable. This aggregated bulk of particles at the surface of membranes leads to partial surface roughness which is more intense for MMMs with higher concentrations of ZIF-8.

It is noteworthy that the roughness of the substrate under the selective layer did not cause any noticeable surface defects in any of the synthesized and modified MMMs. Hence it can be said that the integrity of the selective layer is preserved during the casting process.

3.1.2. XRD Analysis

The X-ray diffraction spectra of (UZ/Pbx-10) and (Z/Pbx-10) samples can be observed in Fig. 4. The distinguishable large peaks from small to large angles belong to the reflection of X-ray from crystal planes at coordination of (100), (200), (211), (220), (310), and (222). They are the peaks that help to characterize ZIF-8 crystals based on previous literature [37]. The comparison of the XRD patterns can lead us to the conclusion that the patterns are very much similar with only minor differences. It shows that the neat ZIF-8 samples are synthesized with significant similarities in the size and shape of the crystal.

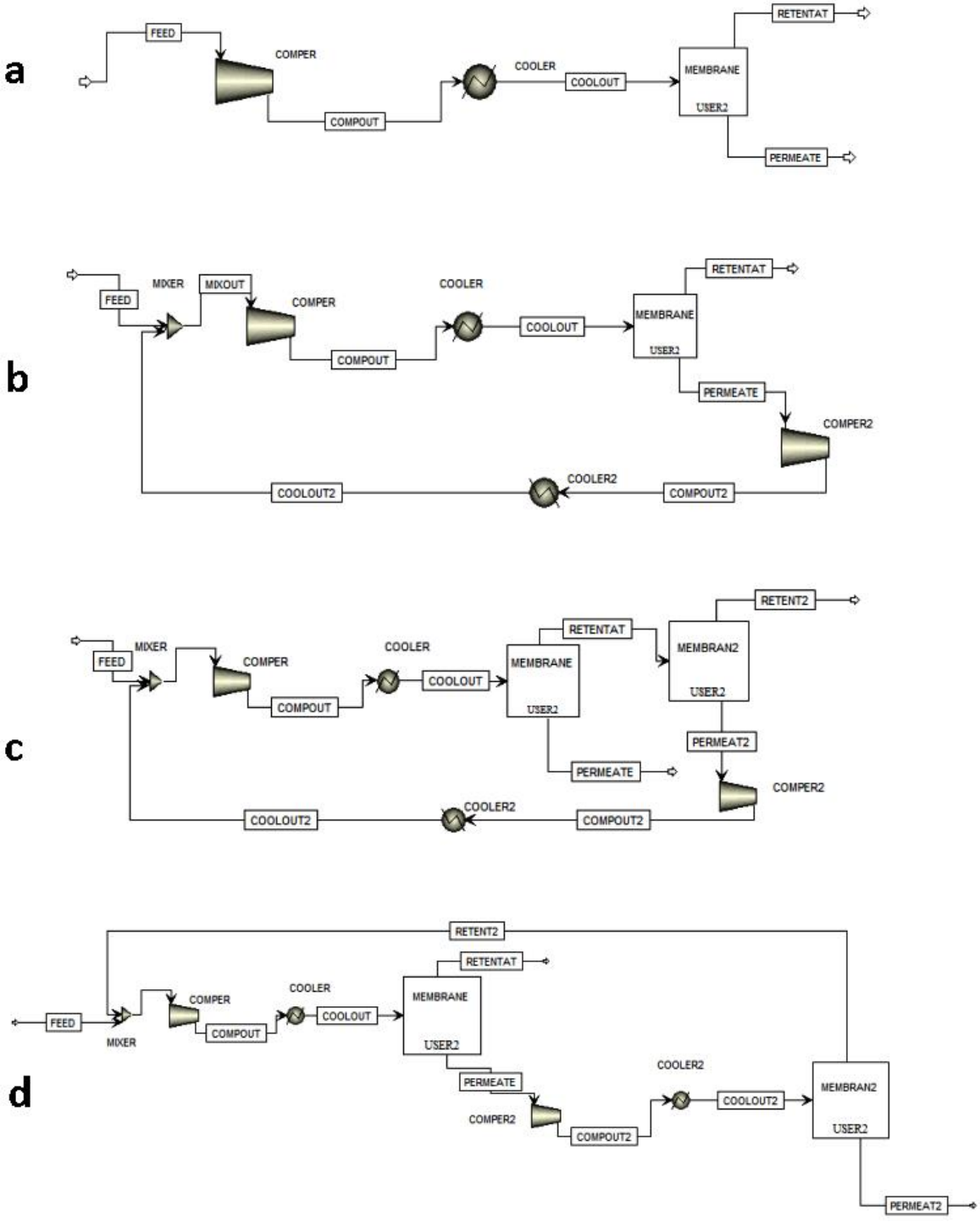

Fig. 1. Process flow diagram of a) single step membrane separation system (SiS), b) single step membrane separation system with recycling of permeate (SiSRP), c) double step membrane separation system with recycling of permeate (DoSRP) and d) double step membrane separation system with recycling of retentate (DoSRR).

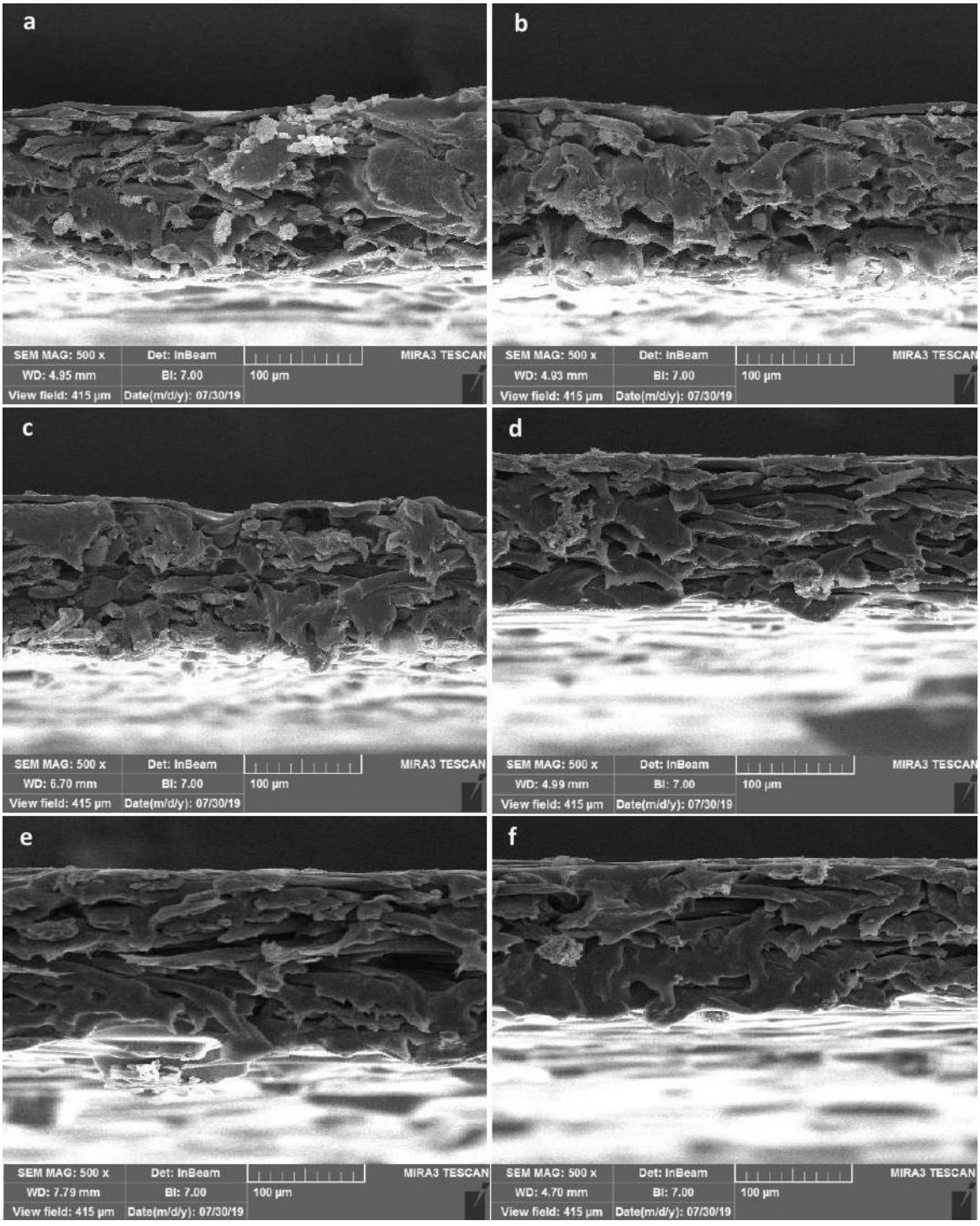

Fig. 2. SEM images from cross-section of a) Z/Pbx-10, b) Z/Pbx-20, c) Z/Pbx-30, d) Z/Pbx-40, e) Z/Pbx-50 and f) Z/Pbx-60.

3.1.3. ^{13}C NMR analysis

To investigate the integrity of the modification of ZIF-8/Pebax 1657 with ionic liquid, spectra of ^{13}C NMR analysis from carefully selected samples have been recorded and presented (Fig. 5 a-d). With the aid of the ^{13}C NMR analysis, it is possible to check the generation of new carbon-carbon bonds in functionalized MMMs. The selection of samples was based on the possibility of clear chemical sift discrimination Fig. 5a, shows the ^{13}C NMR spectra collected from Pebax 1657, ionic liquid (DBMF) and pristine ZIF-8 samples and Fig. 5b, c, d include ^{13}C NMR spectra of (UZ/Pbx-10), (Pbx) and (Z/Pbx-10). The chemical shift positions of investigated samples are provided as supplementary material (see the supplementary file, Table S2). No distinguishable different ^{13}C NMR peak positions can be observed when comparing spectra of (UZ/Pbx-10) and pure Pebax 1657 in Fig. 5a and Fig. 5b, hence it appears that during the synthesis of (UZ/Pbx-10), and unmodified membrane, a new C-C bond did not form. In Fig. 5c, two near peaks recognizable by the blue ring at 122.5 ppm and 125.2 ppm are present in ^{13}C NMR spectrum of (Pbx) sample. These peaks merged into a single peak in Fig. 5a and Fig. 5b, are related to two atoms of carbon in the imidazole group of DBMF which are in identical molecular positions. The minor change in position of chemical shift in spectra of the mentioned atoms of carbon demonstrates that there are electron clouds with different densities around their atom cores. This can be related to the possible interconnection of one carbon atom with its neighboring carbon atom causing the alteration of symmetric electron cloud density of atoms and generation of new chemical shifts in the DMBF spectrum. The identical alteration in chemical shifts can

be seen in Fig. 5d (blue ring). However, in this spectrum, two near peaks at 12.51 and 14.32 ppm, can be distinguished which cannot be observed in other spectrums due to the overlapping (red rings). The change in the position of chemical shift for (Z/Pbx-10) at 12-15 ppm is because of the change in electron cloud density around the core of carbon atom outside the three-carbon ring of imidazole. This observation demonstrates the C-C interconnection between the out of ring carbon atom of the imidazole molecule of ZIF-8 with a carbon atom in DBMF.

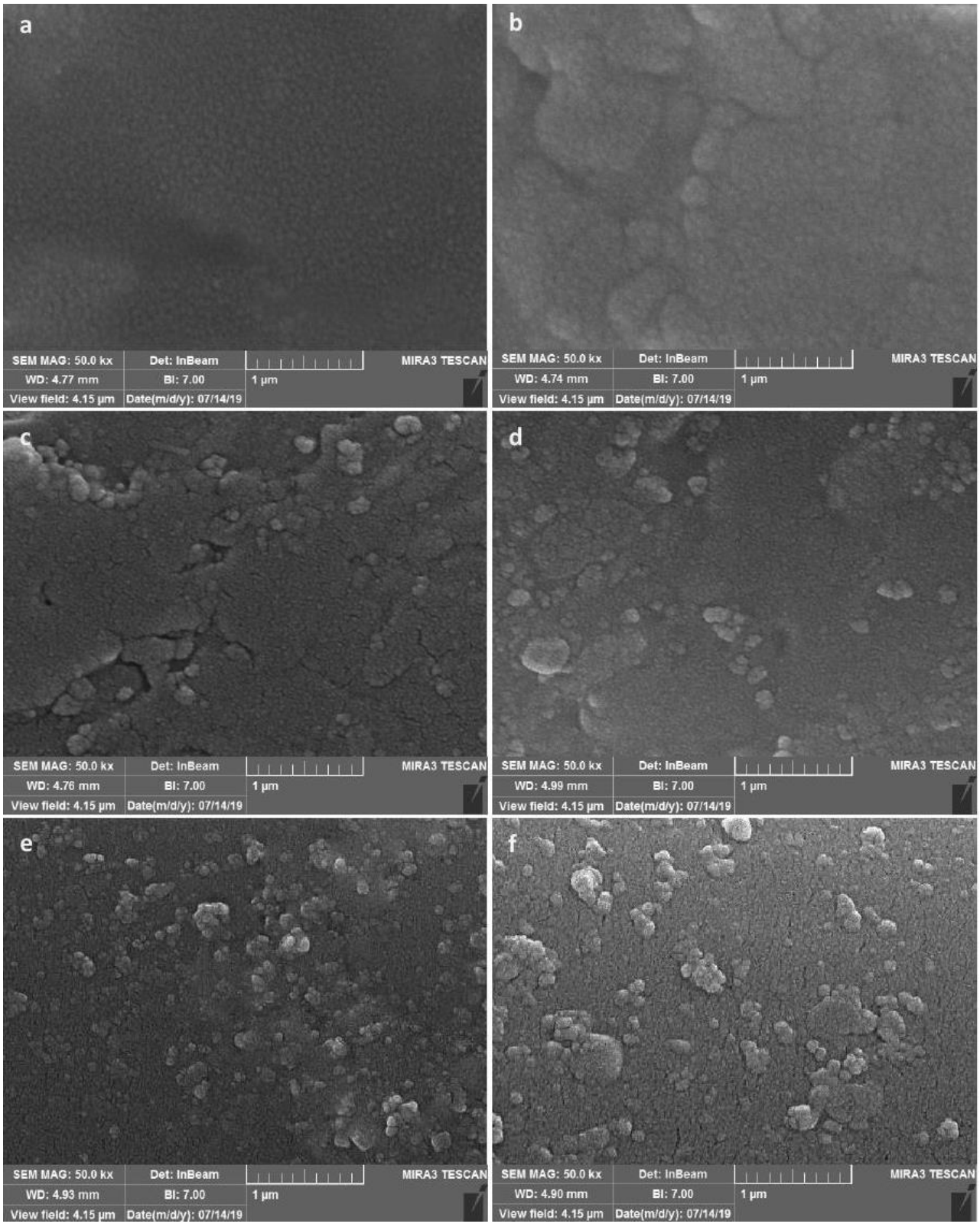

Fig. 3. SEM from the surface of a) Z/Pbx-10, b) Z/Pbx-20, c) Z/Pbx-30, d) Z/Pbx-40, e) Z/Pbx-50 and f) Z/Pbx-60.

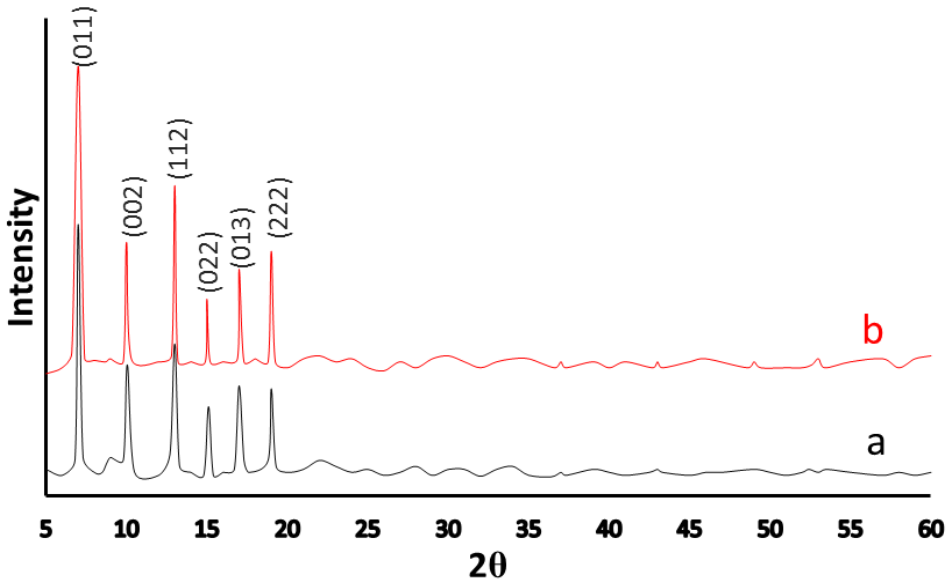

Fig. 4. The XRD pattern of a) (UZ/Pbx-10) and b) (Z/Pbx-10) MMM samples.

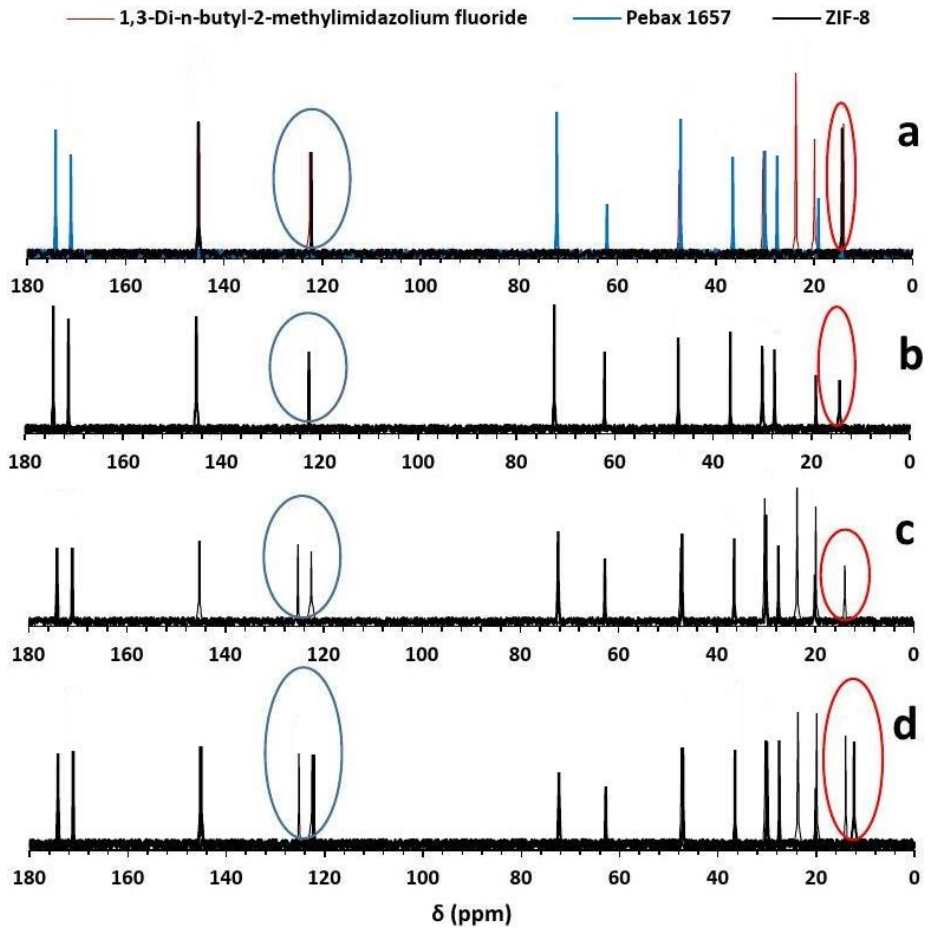

Fig. 5. ^{13}C NMR pattern of a) (dark) ZIF-8, (blue) Pebax and (red) DBMF b) UZ/Pbx-10 c) Pbx and d) Z/Pbx-10 samples.

3.1.4. Permeation analysis

The result of mixed gas tests can be observed in Fig. 6. As can be seen, the CO_2 permeance of IL-modified MMMs at lower concentrations of ZIF-8 (below 30 wt.%) is higher than that of pure Pebax 1657 membrane, however when the concentration of ZIF-8 rises (above 40 wt.%) in the matrix of Pebax 1657, the CO_2 permeance decline. This observation is according to Ordonez et al. [38] report. It is probable that with the rise of ZIF-8 concentration, at lower concentrations the presence of particles in the matrix of polymers leads to disruption of chain packing and fractional free volume increase of the

polymer and accordingly the increase in permeance of all penetrants [39-41]. Moreover, 0.34 nm of pore diameter of ZIF-8 is between the molecular diameters of CO_2 (0.33 nm) and that of CH_4 (0.38 nm), hence the higher concentrations of ZIF-8 normally come to higher sorption of CO_2 and diffusivity and thereafter higher CO_2 permeance. However, at concentrations above 40 wt.%, according to previous works on the polymeric membrane and MMMs [42,43], the polymer matrix is not freely available for gas molecules to pass and the pathways for penetrating gas molecules become longer and more tortuous leading to a noticeable decline in both CO_2 and CH_4 permeances. The CO_2/CH_4 selectivity is higher for all IL-MMMs compared with pure Pebax 1657 membrane and at high concentrations of ZIF-8 (above 40 wt.%), the increase in CO_2/CH_4 selectivity is significant with an increase in ZIF-8 concentration in the synthesis solution. This is related to the abundance of ZIF-8 particles in MMMs with enhanced affinity for CO_2 sorption and remarkable molecular sieving ability which was observed in other works as well [44]. The results of permeation experiments at three different temperatures to achieve activation energy of permeation can be observed in Table S3 (refer to the supplementary file, Table S3). The activation energy of permeation through different synthesized MMMs resulted from exponential data fitting using data sets of Table S3 is presented in Table S4 (also see supplementary file).

The permeation of CO_2 and CH_4 in the synthesized MMMs was based on a combination of a well-known solution-diffusion mechanism in the polymeric phase and surface diffusion and molecular sieving in ZIF phase. Based on the solution-diffusion mechanism, gases dissolve in the Pebax matrix then diffuse through it. Concurrently gases transport through the ZIF phase occur by adsorbing initially into the pores, secondly, diffusion along the surface of the pore happens, and finally, the desorption back to the permeate occurs [45]. The effect of diffusion and adsorption in overall permeation through ZIF is considerable.

Gases absorb into pores of ZIF due to the molecular affinity between gas and adsorbent. In general, molecules that have larger dipole moments have higher heats of adsorption [46]. Thus, the affinity of ZIF for CO_2 is higher compared with conventional industrial gases like N_2 and CH_4. This is because of a higher molecular weight and a stronger quadrupole moment of CO_2. Once gas moves toward pores of ZIF, due to the difference in chemical potential across the membrane, surface diffusion takes place [45,47]. Surface diffusion happens in any pores of different sizes; however, its share is insignificant in large ones which permit gases to evade lattice potential field. Molecules with different sizes diffuse at a different rate in ZIF pores; this is more intense for the molecule that has nearly the same size of the pores. For the case of ZIF-8, the pore size of this MOF is 0.34 nm which is smaller than the kinetic diameter of CH_4 (0.38 nm) and larger than that of CO_2 (0.33nm). If the particle-polymer interfacial incompatibilities are neglected and we assume that the only pores in MMMs belong to ZIF-8, the size of ZIF-8 pores cause the molecular saving to become dominant separation mechanism of CO_2/CH_4 separation case.

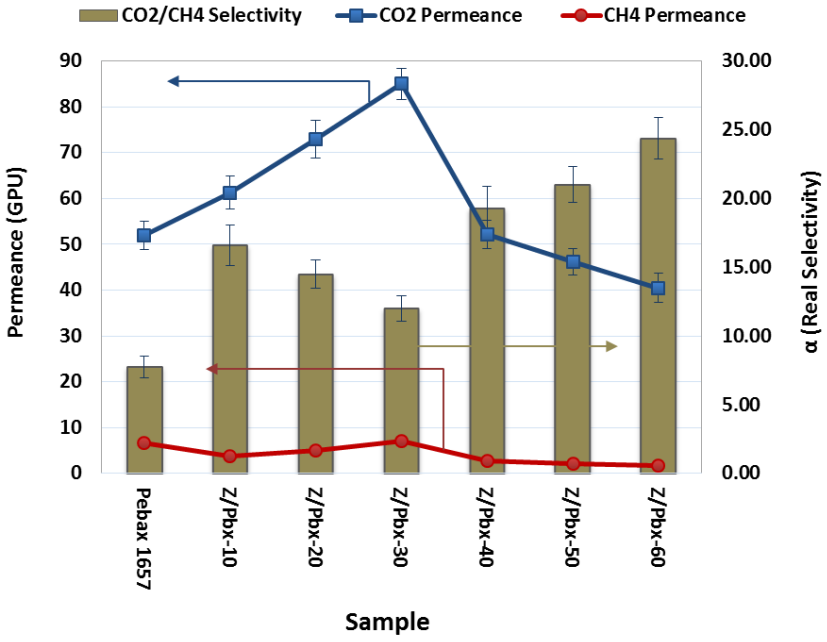

Fig. 6. The permeances of CO_2 and CH_4 along with CO_2/CH_4 selectivity for neat Pebax 1657 membrane and all synthesized MMMs.

3.2. Results and discussions of modeling and simulation parts

The results of the sensitivity analysis of different parameters on CO_2 and CH_4 permeate flow rates in Aspen Plus are presented in Figures 7-11.

3.2.1. The effect of membrane area and module number on the permeate flow rates

The effect of membrane area on CO_2 and CH_4 permeate flow rates of different simulated membrane system configurations (SiS, SiSRP, DoSRP and DoSRR) are presented in Fig.7 a-d.

When comparing subfigures of Fig. 7 with each other, it can be seen that the CO_2 permeate flow of SiSRP and DoSRR at available high membrane areas are significantly higher than those of SiS and DoSRP while this is not the case for CH_4, the reason can be related to the fact that the in SiSRP and DoSRR configurations at high membrane areas, significantly larger mole percentage of exit streams are recycled back to the feed stream compared with SiS and DosRP, hence larger partially purified feed flow rate enters the membrane and therefore CO_2 content increases in permeate flow. However for CH_4 because the recycled stream is partially depleted from CH_4, reduction in permeate flow rate is observed. Non-linear increase in CO_2 flow rate and decrease in CH_4 flow rates with an increase in membrane area for SiSRP and DoSRR cases can also be related to the large recycle rate of these configurations. It is also noteworthy that in system configurations with higher recycle rates (SiSRP and DoSRR), MMMs with higher permeances of gases (Z/Pbx-30, Z/Pbx-20 and Z/Pbx-10) favors high membrane area. This means that for these MMM samples, higher membrane area leads to better separation performance and a larger difference between CO_2 and CH_4 permeate flow rates.

The effect of the number of modules on CO_2 and CH_4 permeate flow rates of simulated membrane system configurations are presented in Fig. S2 (see supplementary file). For all synthesized MMMs. The effect of the number of modules on permeate flow rates of gases is very similar to the effect of the increase in membrane area. This was anticipated because the increase in module numbers leads to the increase in available membrane area for permeation of gases, hence their effect on the flow rate of gases in

permeate must be identical. However, the effect of the increase in membrane area on permeate flow rates is significantly more intense than that of the number of modules. One reason for that is related to the fact that modules used in this study were both flat with very limited area for permeation of gases. Hence very large numbers of modules are required to achieve a membrane area for a significant increase in permeate flow rate. Similar to sensitivity analysis of membrane area, in this case, it can be seen that the higher numbers of modules are favored by high permeable MMM samples (Z/Pbx-30, Z/Pbx-20 and Z/Pbx-10) in SiSRP and DoSRR. These samples show poor separation performance at lower numbers of modules compared with Z/Pbx-40, Z/Pbx-50, and Z/Pbx-60 samples, however, as the module numbers increase, the CO_2 permeate flow rate boosts while the rate of CH_4 flow rate increment declines substantially leading to the enhancement in CO_2/CH_4 separation performance of the whole system configuration.

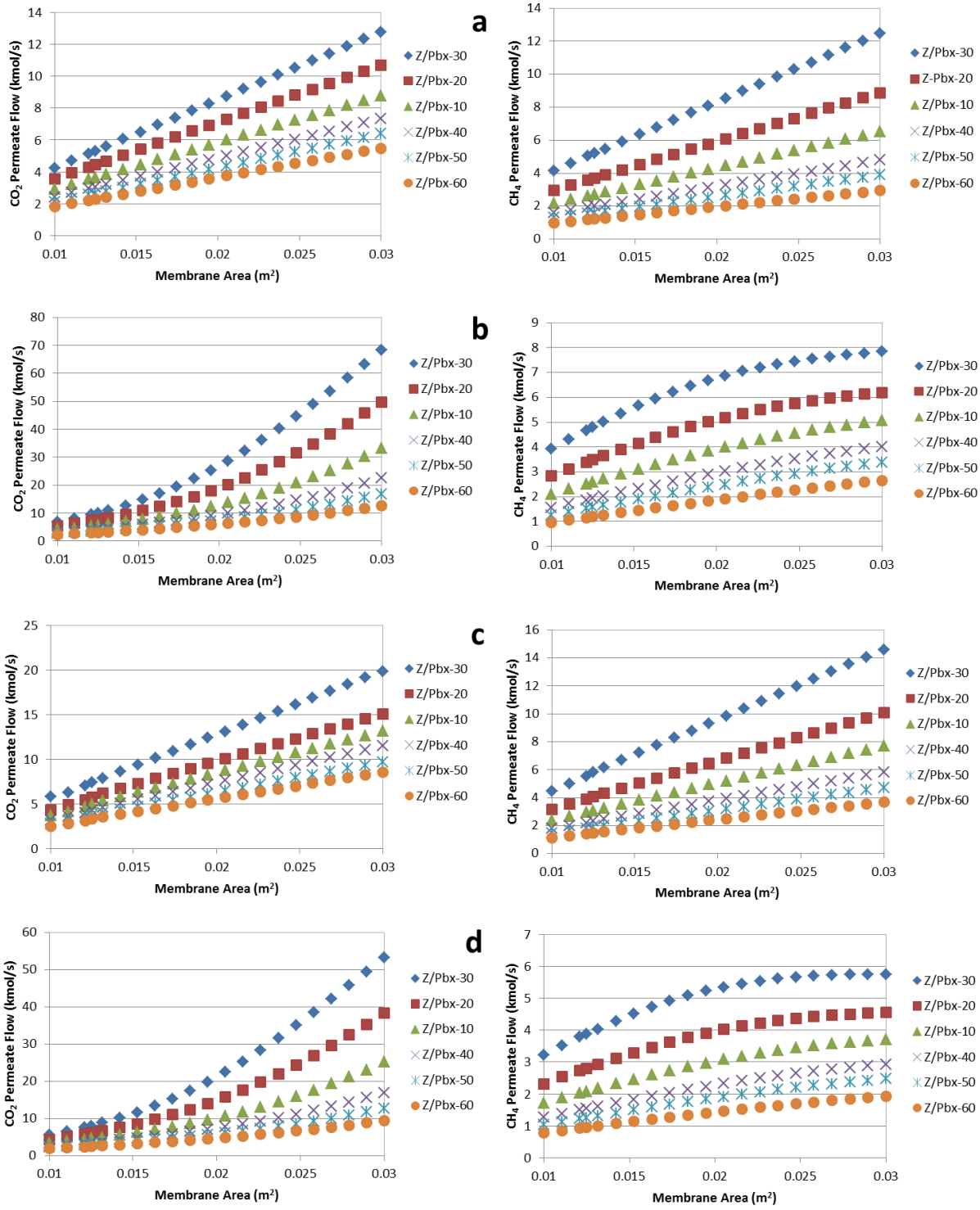

Fig. 7. The simulated effect of membrane area on CO_2 and CH_4 permeate flow rates in: a) SiS, b) SiSRP, c) DoSRP, and d) DoSRR membrane system configurations for all synthesized MMMs.

3.2.2. The effect of pressure difference across membrane on the permeate flow rates

The effect of pressure difference across membranes on CO_2 and CH_4 permeate flow rates of simulated membrane system configurations are presented in Fig.8 a-d for all synthesized MMMs. As can be seen with the increase in applied feed pressure or equivalently the pressure difference across the membrane the permeate flow rates of CO_2 and CH_4 increase. This was due to the increase in gas flux which is directly related to the increasing pressure difference across the membrane. As can be observed the changing trend of CO_2 permeate flow rate of all of MMMs in four different configurations show increasing slope with an increase in applied pressure difference and this leads to enhancement in separation performance in all configurations in higher pressure differences. Moreover, the increased permeance of MMMs with increased pressure difference across membranes leads to an increase in CH_4 recovery of the membrane system especially for systems utilizing permeate recycle stream due to the overall gas permeation enhancement [48]. For the case of DoSRR configuration which utilizes retentate recycle an intense increase in CO_2 is observed which is not typical of systems with retentate recycle. This is because the permeate of the first step of membrane separation enters the second step, therefore the retentate of the second step of DoSRR composed of relatively high concentration of CO_2 leading to an increase in CO_2 concentration of feed stream which then results in a significant increase in CO_2 permeate flux.

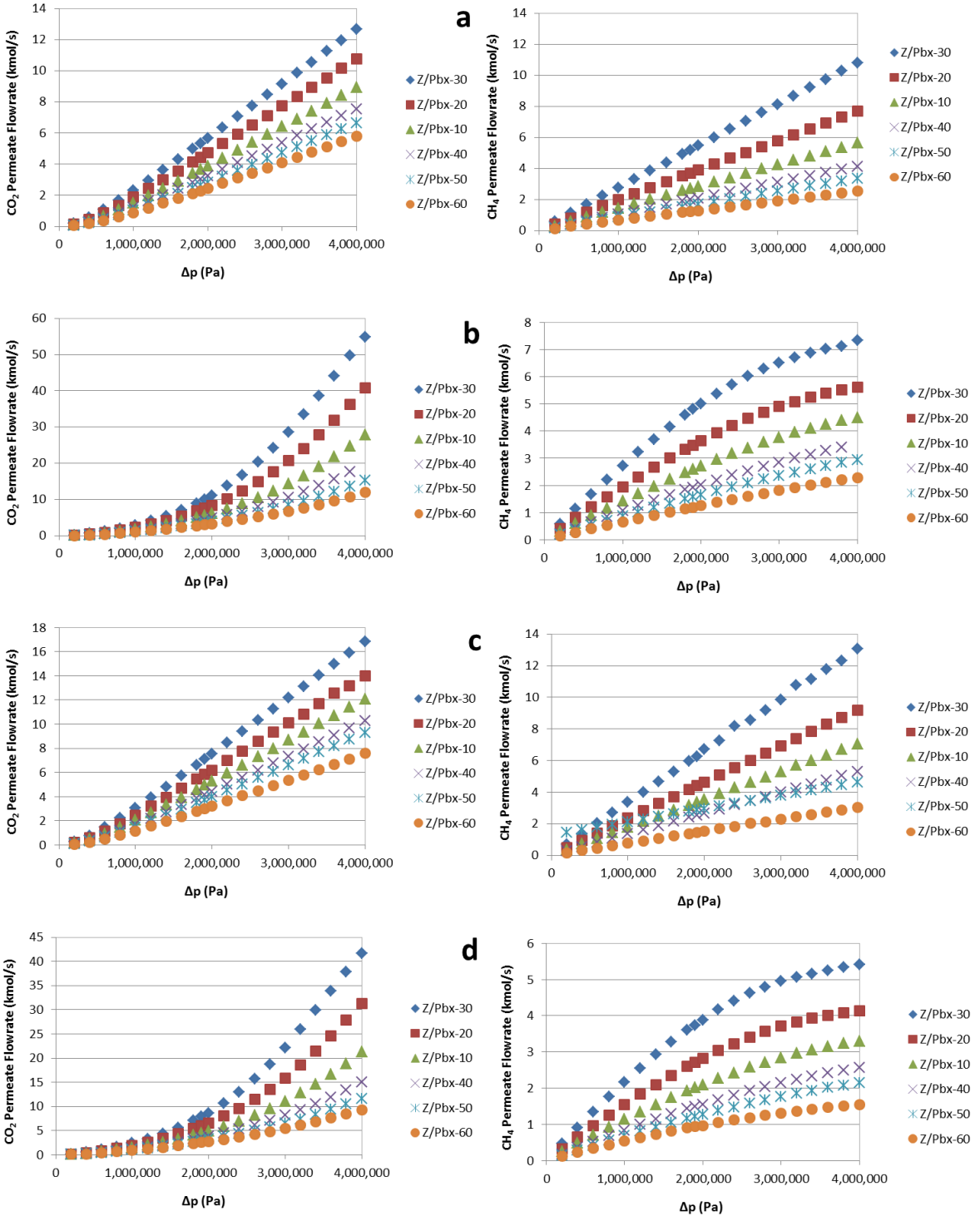

Fig. 8. The simulated effect of pressure difference across membranes on CO_2 and CH_4 permeate flow rates in: a) SiS, b) SiSRP, c) DoSRP and d) DoSRR membrane system configurations for all synthesized MMMs.

3.2.3. The effect of membrane feed composition on the permeate flow rates

The effect of feed composition on CO_2 and CH_4 permeate flow rates of simulated membrane system configurations are presented in Fig. 9 a-d for all synthesized MMMs. With an increase in the CH_4 content of the feed, in all different configurations, the CO_2 permeate flow rate decreases while CH_4 permeate flow rate increases. The decrease in the CO_2 flow rate is more drastic than the increase in CH4 flow rate. This is because all of the synthesized and modeled MMMs in this study are strong CO_2 selective membranes, hence the decrease in the CO_2 content of the feed affects more on CO_2 permeation than CH_4 permeation. Moreover, the increase of CH_4 content of the feed from 80% to near 100% means near 25% increase in CH_4 feed content, however for the case of CO_2 the decrease of CO_2 content in the feed from 20% to near zero means almost 100% decrease in CO_2 feed content. This can be another reason for the significant decline in CO_2 permeate flow rate and a mild increase in CH_4 permeate flow rate.

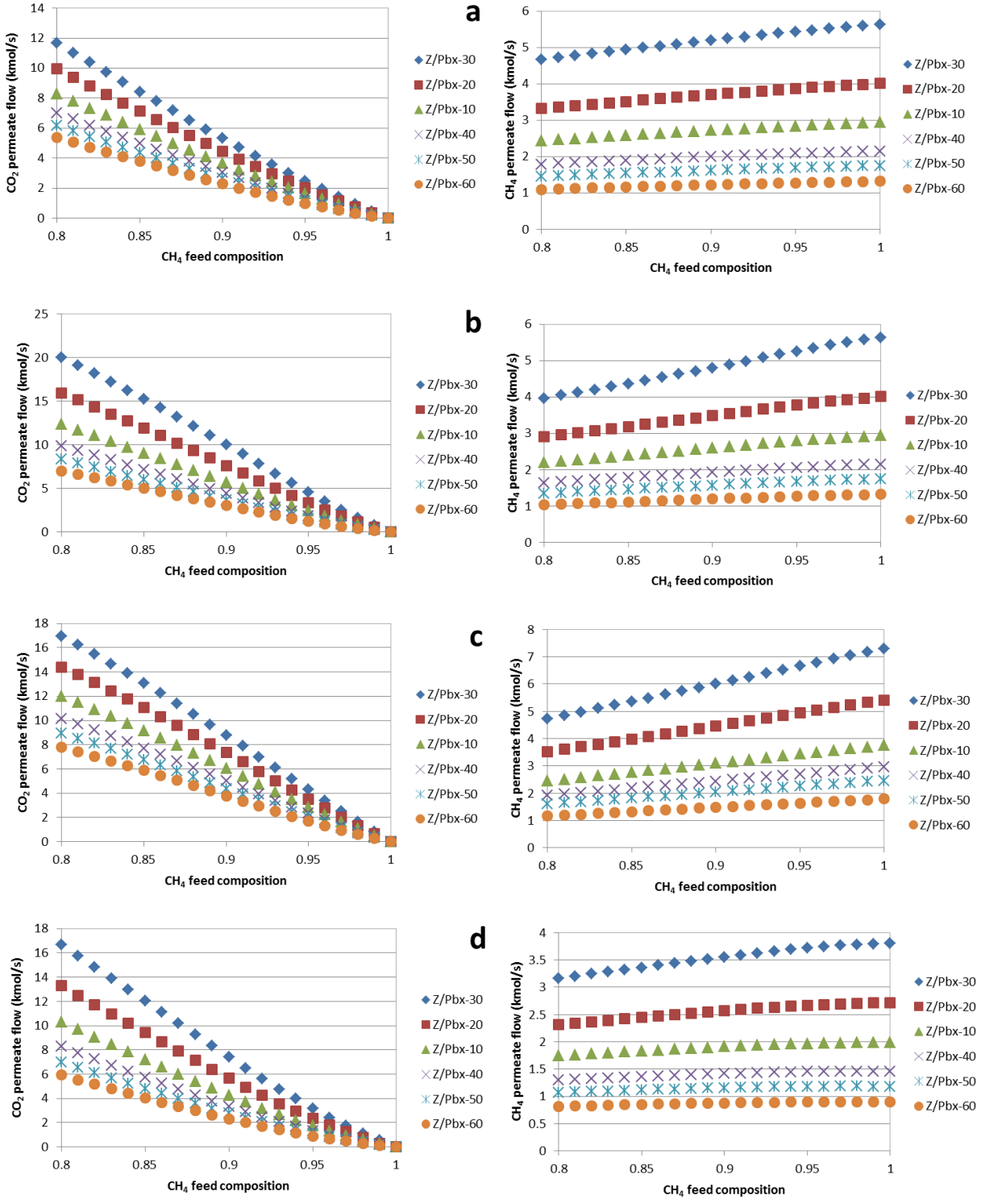

Fig. 9. The simulated effect membrane feed composition on CO_2 and CH_4 permeate flow rates in: a) SiS, b) SiSRP, c) DoSRP and d) DoSRR membrane system configurations for all MMMs.

It is also noteworthy that at CH_4 feed content near 100%, the highest CH_4 recovery obtains from DoSRP and while DoSRR shows the lowest CH_4 recovery. It means that when the feed is almost pure CH_4, DoSRP is the favorable configuration and DoSRR is the least desirable configuration. The reason can be related to the fact that when membrane area is relatively low (0.0125 m^2) and the number of modules is limited (1,000,000) the configurations with permeate recycle (e.g.: DoSRP) show better separation performance and CH_4 recovery since larger amounts of CH_4 is recycled back to the feed [49]. This can be observed in sensitivity analysis related to membrane area and the number of modules (Fig. 7 and Fig. S2) at low values of their horizontal axis. Another important point in Fig. 9 is that when comparing all four subsections of this figure it can be concluded that at high CH_4 content in the feed, the MMMs with lower CO_2/CH_4 selectivity and higher permeances are favored. As can be seen, the highest CH_4 permeate flow rates in all configurations belong to (Z/Pbx-30) sample with the highest permeances for both CO_2 and CH_4 and lowest CO_2/CH_4 selectivity.

3.2.4. The temperature effect on the permeate flow rates

The effect of temperature on CO_2 and CH_4 permeate flow rates of simulated membrane system configurations are presented in Fig.10 a-d for all synthesized MMMs. As can be seen, the rise in temperature increased both CO_2 and CH_4 permeate flow rates for all investigated MMMs in all system configurations. This was mainly due to the significantly increased flexibility of PEO chains in the Pebax 1657 matrix which provides excess fractional free volume for CO_2 and CH_4 to diffuse leading to an increase in permeance of all MMMs [6].

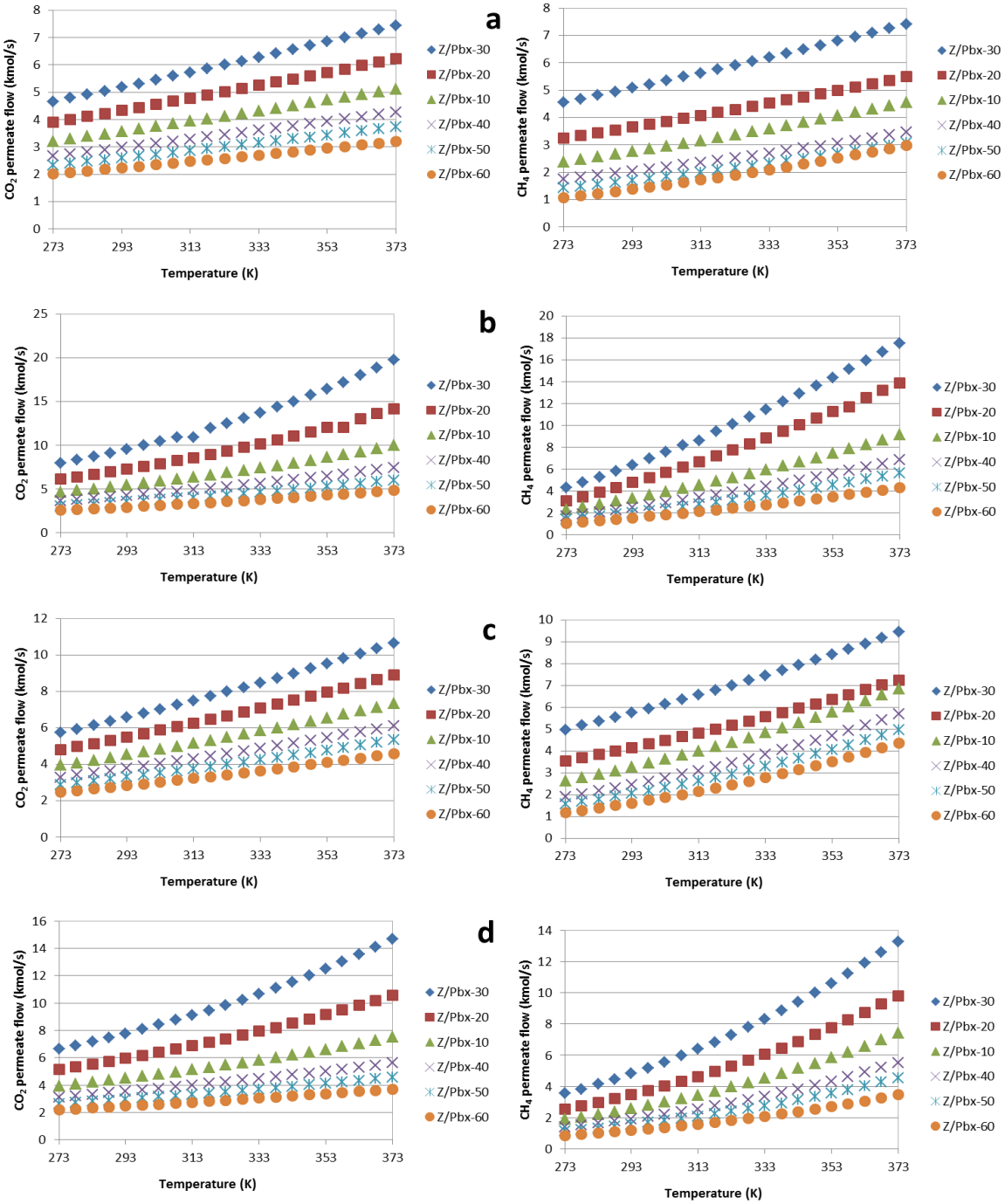

Fig. 10. The simulated effect temperature on CO_2 and CH_4 permeate flow rates in: a) SiS b) SiSRP, c) DoSRP and d) DoSRR membrane system configurations for all synthesized MMMs.

Moreover, as can be seen, the slope of change in CO_2 and CH_4 flow rates with temperature is higher for more permeable and less selective MMMs. The reason was that based on eq. (8) and Table S3, the permeance of MMMs with larger values of E_p is more affected by temperature variations. Hence more sensible MMMs to temperature are MMMs with larger E_p value. This is in good agreement with the results presented in Fig. 10 a-d. It is worth mentioning that the separation performance of all system configurations for all MMMs notably deteriorated with an increase in temperature. In fact, in 373 K, the value of CH_4 permeate flow rate approaches the CO_2 permeate flow rate value for most of the MMMs samples simulated meaning that at temperatures as high as 373 K, the separation performance of membranes and therefore different configurations of membrane systems decline substantially leading the membrane separation systems to become futile.

3.2.5. The effect of membrane thickness on the permeate flow rates

The effect of membrane thickness on CO_2 and CH_4 permeate flow rates of simulated membrane system configurations are presented in Fig.11 a-d for all synthesized MMMs.

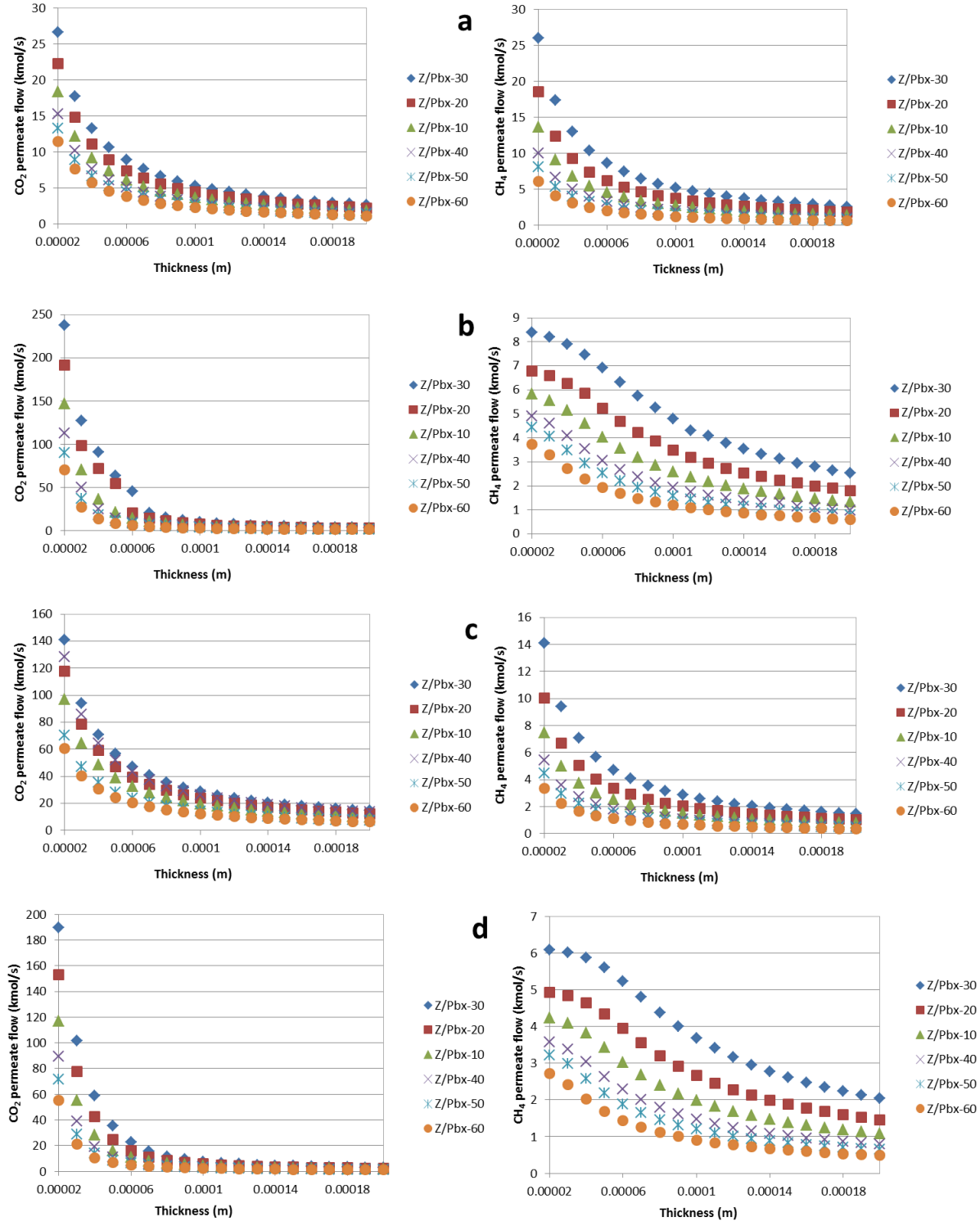

Fig. 11. The simulated effect membrane thickness on CO_2 and CH_4 permeate flow rates in: a) SiS, b) SiSRP, c) DoSRP and d) DoSRR membrane system configurations for all synthesized MMMs.

With an increase in the thickness of MMMs the CO_2 permeate flow rate drastically declines for all MMMs in all four different configurations. This is related to the fact that the increase in the thickness of membranes leads to decrease in permeance of both CO_2 and CH_4 which is observable, however, because all MMMs in this study are strongly CO_2 selective membrane the effect of membrane thickness is more intense on CO_2 then CH_4 permeate flow. Moreover, the increase of thickness from 20 µm to 60 µm means 200% increase in thickness while the increase of thickness from 60 µm to 100 µm means 67% increase in the thickness of MMMs and this percentage decreases substantially when the thickness increases gradually, therefore the gas flux change at lower thicknesses are remarkably more intense than that at higher thicknesses. When comparing subfigures of Fig. 11 with each other it can be concluded that the separation of CO_2 from CH_4 ability of SiSRP, DoSRP and DoSRR configurations are noticeably superior to that of SiS configuration. The reason can be related to the presence of a recycle stream with different rates in SiSRP, DoSRP and DoSRR configurations which provide the more purified product by re-purification of permeate or retentate streams. It is also important to mention that when the MMMs are fabricated with the minimum possible thickness, more permeable membranes are more efficient in system configurations with recycles; however when the thickness of MMMs increases the separation performance declines and the more selective MMMs become more efficient in these systems. It can be concluded from this sensitivity analysis that to reach superior separation performance in different configurations, first, the membrane in modules has to be as thin as possible provided that its morphological integrity preserves, second the recycle of permeate or retentate must be applied to the membrane separation system.

4. Conclusions

ZIF-8 particles have been synthesized with a high molar ratio of $MeIM/Zn(NO_3)_2$. $6(H_2O)=32$. These particles have been introduced in the matrix of modified Pebax 1657 with concentrations up to 60 wt.%. Di-butyl-methylimidazolium fluoride (DBMF) was used to functionalize the surface of Pebax 1657 for enhancement of compatibility between ZIF-8 and Pebax 1657. The results of ^{13}C-NMR analysis suggested that there are possible new carbon-carbon bonds at the interface of ZIF-8 and functionalized Pebax 1657. The SEM micrographs from the surface of synthesized MMMs visually approved the integrity of the selective layer. The CO_2/CH_4 binary mixed gas test results showed the successful incorporation of high concentrations of ZIF-8 in the matrix of Pebax 1657. The membrane containing 60 wt. % of ZIF-8, showed the highest CO_2/CH_4 selectivity with a significant decline in CO_2 permeance while the sample having 30 wt. % of ZIF-8, showed the lowest selectivity and highest CO_2 permeance among all synthesized cases. The results overly demonstrate significant improvement of MMMs performance compared with Pebax 1657 pure membrane. The results of membrane separation system configurations modeling in Microsoft Excel and its linked simulation with Aspen Plus showed that the increase in membrane area, number of membrane modules and the pressure difference across membranes lead to increase of CO_2 permeate flow with elevating slope for SiSRP and DoSRR configurations of membrane separation systems resulting in CO_2/CH_4 separation enhancement for these two configurations compared with SiS and DoSRP. This was mainly due to the relatively larger recycle rate in SiSRP and DoSRR. The sensitivity analysis of membrane feed composition on permeate flow of gases showed that nearly pure CH_4 feed the leads to the observation of highest CH_4 recovery from DoSRP and while DoSRR shows the lowest CH_4 recovery because of the limitations of membrane area and module number in Aspen Plus simulation. The rise in temperature showed notable increasing effect on permeates flow rates of both gases leading to the deterioration of separation effectiveness of all membrane system configurations. Finally, the results of the sensitivity analysis of membrane thickness on permeate flow rates of gases showed that synthesis of thinner membranes leads to better separation performance as long as the integrity of the membrane preserves. Moreover, utilizing permeate or retentate recycle lead to more purified product.

Acknowledgments

We acknowledge the Petroleum University of Technology (PUT) due to its collaboration in providing facilities for the experimental part of this study.

Declaration of interests

We declare that there are no competing interests in this work.

References

[1] S. Nesic, Effects of multiphase flow on internal CO_2 corrosion of mild steel pipelines, Energy Fuels, 26 (2012) 4098-4111. https://doi.org/10.1021/ef3002795.

[2] B. Paschke, A. Kather, Corrosion of pipeline and compressor materials due to impurities in separated $_{CO2}$ from fossil-fuelled power plants, Energy Procedia, 23 (2012) 207-215. https://doi.org/10.1016/j.egypro.2012.06.030.

[3] M. Wu, S. Wang, H. Liu, A study on inhibitors for the prevention of hydrate formation in gas transmission pipeline, J. Nat. Gas Sci. Eng., 16 (2007) 81-85. https://doi.org/10.1016/s1003-9953(07)60031-0.

[4] J. Gomes, S. Santos, J. Bordado, Choosing amine-based absorbents for CO_2 capture, Environ. Technol., 36 (2015) 19-25. https://doi.org/10.1080/09593330.2014.934742.

[5] C. Song, Q. Liu, S. Deng, H. Li, Y. Kitamura, Cryogenic-based CO_2 capture technologies: State-of-the-art developments and current challenges, Renewable Sustainable Energy Rev., 101 (2019) 265-278. https://doi.org/10.1016/j.rser.2018.11.018.

[6] A. Jomekian, R.M. Behbahani, T. Mohammadi, A. Kargari, High speed spin coating in fabrication of Pebax 1657 based mixed matrix membrane filled with ultra-porous ZIF-8 particles for CO 2/CH 4 separation, Korean J. Chem. Eng., 34 (2017) 440-453. https://doi.org/10.1007/s11814-016-0269-1.

[7] W. Fam, J. Mansouri, H. Li, V. Chen, Improving CO_2 separation performance of thin film composite hollow fiber with Pebax® 1657/ionic liquid gel membranes, J. Membr. Sci., 537 (2017) 54-68. https://doi.org/10.1016/j.memsci.2017.05.011.

[8] J. Kim, Q. Fu, K. Xie, J.M. Scofield, S.E. Kentish, G.G. Qiao, CO_2 separation using surface-functionalized SiO2 nanoparticles incorporated ultra-thin film composite mixed matrix membranes for post-combustion carbon capture, J. Membr. Sci., 515 (2016) 54-62. https://doi.org/10.1016/j.memsci.2016.05.029.

[9] A. Jomekian, B. Bazooyar, R.M. Behbahani, T. Mohammadi, A. Kargari, Ionic liquid-modified Pebax® 1657 membrane filled by ZIF-8 particles for separation of CO_2 from CH_4, N_2 and H_2, J. Membr. Sci., 524 (2017) 652-662. https://doi.org/10.1016/j.memsci.2016.11.065.

[10] W. Fam, J. Mansouri, H. Li, J. Hou, V. Chen, Effect of inorganic salt blending on the CO_2 separation performance and morphology of Pebax® 1657/ionic liquid gel membranes, Ind. Eng. Chem. Res., (2019) 3304-3313. https://doi.org/10.1021/acs.iecr.8b05027.s001.

[11] E. Ghasemi Estahbanati, M. Omidkhah, A. Ebadi Amooghin, Interfacial design of ternary mixed matrix membranes containing Pebax 1657/silver-nanopowder/[BMIM][BF_4] for improved CO_2 separation performance, ACS Appl. Mater. Interfaces, 9 (2017) 10094-10105. https://doi.org/10.1021/acsami.6b16539.

[12] S. Meshkat, S. Kaliaguine, D. Rodrigue, Mixed matrix membranes based on amine and non-amine MIL-53 (Al) in Pebax® MH-1657 for CO_2 separation, Sep. Purif. Technol., 200 (2018) 177-190. https://doi.org/10.1016/j.seppur.2018.02.038.

[13] M. Mozafari, R. Abedini, A. Rahimpour, Zr-MOFs-incorporated thin film nanocomposite Pebax 1657 membranes dip-coated on polymethylpentyne layer for efficient separation of CO_2/CH_4, J. Mater. Chem. A, 6 (2018) 12380-12392. https://doi.org/10.1039/c8ta04806a.

[14] G. Dong, J. Hou, J. Wang, Y. Zhang, V. Chen, J. Liu, Enhanced CO_2/N_2 separation by porous reduced graphene oxide/Pebax mixed matrix membranes, J. Membr. Sci., 520 (2016) 860-868. https://doi.org/10.1016/j.memsci.2016.08.059.

[15] D. Zhao, J. Ren, Y. Wang, Y. Qiu, H. Li, K. Hua, X. Li, J. Ji, M. Deng, High CO_2 separation performance of Pebax®/CNTs/GTA mixed matrix membranes, J. Membr. Sci., 521 (2017) 104-113. https://doi.org/10.1016/j.memsci.2016.08.061.

[16] P. Bernardo, J.C. Jansen, F. Bazzarelli, F. Tasselli, A. Fuoco, K. Friess, P. Izák, V. Jarmarová, M. Kačírková, G. Clarizia, Gas transport properties of Pebax®/room temperature ionic liquid gel membranes, Sep. Purif. Technol., 97 (2012) 73-82. https://doi.org/10.1016/j.seppur.2012.02.041.

[17] H. Rabiee, A. Ghadimi, T. Mohammadi, Gas transport properties of reverse-selective poly (ether-b-amide6)/[Emim][BF4] gel membranes for CO_2/light gases separation, J. Membr. Sci., 476 (2015) 286-302. https://doi.org/10.1016/j.memsci.2014.11.037.

[18] K.-B. Wang, Q. Xun, Q. Zhang, Recent progress in metal-organic frameworks as active materials for supercapacitors, EnergyChem, 2 (2020) 100025. https://doi.org/10.1016/j.enchem.2019.100025.

[19] Z. Wu, J. Xie, Z.J. Xu, S. Zhang, Q. Zhang, Recent progress in metal–organic polymers as promising electrodes for lithium/sodium rechargeable batteries, Journal of Materials Chemistry A, 7 (2019) 4259-4290.

[20] G. Xiao, T. Geng, B. Zou, Emerging Functional Materials under High Pressure toward Enhanced Properties, ACS Materials Letters, 2 (2020) 1233-1239.

[21] D.-L. Chen, N. Wang, F.-F. Wang, J. Xie, Y. Zhong, W. Zhu, J.K. Johnson, R. Krishna, Utilizing the Gate-Opening Mechanism in ZIF-7 for Adsorption Discrimination between N_2O and CO_2, J. Phys. Chem. C, 118 (2014) 17831-17837. https://doi.org/10.1021/jp5056733.

[22] T. Li, Y. Pan, K.-V. Peinemann, Z. Lai, Carbon dioxide selective mixed matrix composite membrane containing ZIF-7 nano-fillers, J. Membr. Sci., 425-426 (2013) 235-242. https://doi.org/10.1016/j.memsci.2012.09.006.

[23] J. van den Bergh, C. Gücüyener, E.A. Pidko, E.J.M. Hensen, J. Gascon, F. Kapteijn, Understanding the Anomalous Alkane Selectivity of ZIF-7 in the Separation of Light Alkane/Alkene Mixtures, Chem. Eur. J., 17 (2011) 8832-8840. https://doi.org/10.1002/chem.201100958.

[24] X. Wu, M. Niknam Shahrak, B. Yuan, S. Deng, Synthesis and characterization of zeolitic imidazolate framework ZIF-7 for CO_2 and CH_4 separation, Microporous

Mesoporous Mater., 190 (2014) 189-196. https://doi.org/10.1016/j.micromeso.2014.02.016.

[25] L. Xiang, L. Sheng, C. Wang, L. Zhang, Y. Pan, Y. Li, Amino-Functionalized ZIF-7 Nanocrystals: Improved Intrinsic Separation Ability and Interfacial Compatibility in Mixed-Matrix Membranes for CO_2/CH_4 Separation, Adv. Mater., 29 (2017) 1606999. https://doi.org/10.1002/adma.201606999.

[26] Y. Ban, Z. Li, Y. Li, Y. Peng, H. Jin, W. Jiao, A. Guo, P. Wang, Q. Yang, C. Zhong, W. Yang, Confinement of Ionic Liquids in Nanocages: Tailoring the Molecular Sieving Properties of ZIF-8 for Membrane-Based CO_2 Capture, Angew. Chem. Int. Ed., 54 (2015) 15483-15487. https://doi.org/10.1002/anie.201505508.

[27] L. Hao, P. Li, T. Yang, T.-S. Chung, Room temperature ionic liquid/ZIF-8 mixed-matrix membranes for natural gas sweetening and post-combustion CO_2 capture, J. Membr. Sci., 436 (2013) 221-231. https://doi.org/10.1016/j.memsci.2013.02.034.

[28] H. Li, L. Tuo, K. Yang, H.-K. Jeong, Y. Dai, G. He, W. Zhao, Simultaneous enhancement of mechanical properties and CO_2 selectivity of ZIF-8 mixed matrix membranes: Interfacial toughening effect of ionic liquid, J. Membr. Sci., 511 (2016) 130-142. https://doi.org/10.1016/j.memsci.2016.03.050.

[29] S.N. Wijenayake, N.P. Panapitiya, S.H. Versteeg, C.N. Nguyen, S. Goel, K.J. Balkus, I.H. Musselman, J.P. Ferraris, Surface Cross-Linking of ZIF-8/Polyimide Mixed Matrix Membranes (MMMs) for Gas Separation, Ind. Eng. Chem. Res., 52 (2013) 6991-7001. https://doi.org/10.1021/ie400149e.

[30] R. Rautenbach, R. Knauf, A. Struck, J. Vier, Simulation and design of membrane plants with AspenPlus, Chem. Eng. Technol., 19 (1996) 391-397. https://doi.org/10.1002/ceat.270190502.

[31] R.A. Davis, Simple gas permeation and pervaporation membrane unit operation models for process simulators, Chem. Eng. Technol., 25 (2002) 717-722. https://doi.org/10.1002/1521-4125(20020709)25:7%3C717::aid-ceat717%3E3.0.co;2-n.

[32] M.H. Murad Chowdhury, X. Feng, P. Douglas, E. Croiset, A new numerical approach for a detailed multicomponent gas separation membrane model and AspenPlus simulation, Chem. Eng. Technol., 28 (2005) 773-782. https://doi.org/10.1002/ceat.200500077.

[33] C. Pan, Gas separation by high flux, asymmetric hollow fiber membrane, AIChE J., 32 (1986) 2020-2027. https://doi.org/10.1002/aic.690321212.

[34] A. Hussain, M.-B. Hägg, A feasibility study of CO_2 capture from flue gas by a facilitated transport membrane, J. Membr. Sci., 359 (2010) 140-148. https://doi.org/10.1016/j.memsci.2009.11.035.

[35] A. Jomekian, R. Behbahani, T. Mohammadi, A. Kargari, Utilization of Pebax 1657 as structure directing agent in fabrication of ultra-porous ZIF-8, J. Solid State Chem., 235 (2016) 212-216. https://doi.org/10.1016/j.jssc.2016.01.004.

[36] M. Mubashir, Y.F. Yeong, K.K. Lau, T.L. Chew, J. Norwahyu, Efficient CO_2/N_2 and CO2/CH4 separation using NH2-MIL-53 (Al)/cellulose acetate (CA) mixed matrix membranes, Sep. Purif. Technol., 199 (2018) 140-151. https://doi.org/10.1016/j.seppur.2018.01.038.

[37] H.-Y. Cho, J. Kim, S.-N. Kim, W.-S. Ahn, High yield 1-L scale synthesis of ZIF-8 via a sonochemical route, Microporous Mesoporous Mater., 169 (2013) 180-184. https://doi.org/10.1016/j.micromeso.2012.11.012.

[38] M.J.C. Ordoñez, K.J. Balkus, J.P. Ferraris, I.H. Musselman, Molecular sieving realized with ZIF-8/Matrimid® mixed-matrix membranes, J. Membr. Sci., 361 (2010) 28-37. https://doi.org/10.1016/j.memsci.2010.06.017.

[39] J. Ahn, W.-J. Chung, I. Pinnau, M.D. Guiver, Polysulfone/silica nanoparticle mixed-matrix membranes for gas separation, J. Membr. Sci., 314 (2008) 123-133. https://doi.org/10.1016/j.memsci.2008.01.031.

[40] S. Matteucci, V.A. Kusuma, S.D. Kelman, B.D. Freeman, Gas transport properties of MgO filled poly (1-trimethylsilyl-1-propyne) nanocomposites, Polymer, 49 (2008) 1659-1675. https://doi.org/10.1016/j.polymer.2008.01.004.

[41] T. Merkel, B.D. Freeman, R. Spontak, Z. He, I. Pinnau, P. Meakin, A. Hill, Sorption, transport, and structural evidence for enhanced free volume in poly (4-methyl-2-pentyne)/fumed silica nanocomposite membranes, Chem. Mater., 15 (2003) 109-123. https://doi.org/10.1021/cm020672j.

[42] M. Sadeghi, M.A. Semsarzadeh, H. Moadel, Enhancement of the gas separation properties of polybenzimidazole (PBI) membrane by incorporation of silica nano particles, J. Membr. Sci., 331 (2009) 21-30. https://doi.org/10.1016/j.memsci.2008.12.073.

[43] G. Van Amerongen, Diffusion in elastomers, Rubber Chem. Technol., 37 (1964) 1065-1152. https://doi.org/10.5254/1.3540396.

[44] S.R. Venna, M.A. Carreon, Highly permeable zeolite imidazolate framework-8 membranes for CO_2/CH_4 separation, J. Am. Chem. Soc, 132 (2010) 76-78. https://doi.org/10.1021/ja909263x.

[45] T. Masuda, N. Fukumoto, M. Kitamura, S.R. Mukai, K. Hashimoto, T. Tanaka, T. Funabiki, Modification of pore size of MFI-type zeolite by catalytic cracking of silane and application to preparation of H_2-separating zeolite membrane, Microporous Mesoporous Mater., 48 (2001) 239-245. https://doi.org/10.1016/s1387-1811(01)00358-4.

[46] F. Eder, M. Stockenhuber, J. Lercher, Sorption of light alkanes on H-ZSM5 and H-mordenite, in: Stud Surf Sci Catal., Elsevier, 1995, pp. 495-500. https://doi.org/10.1021/jacs.7b12901.s001.

[47] S.V. Sotirchos, V.N. Burganos, Transport of gases in porous membranes, MRS Bulletin, 24 (1999) 41-45. https://doi.org/10.1557/s0883769400051903.

[48] W.J. Schell, H. CD, Spiral-wound permeators for purification and recovery, Che. Eng. Prog., 13 (1982) 33-37. http://pascal-francis.inist.fr/vibad/index.php?action=getRecordDetail&idt=PASCAL83X0039813

[49] R. Qi, M.A. Henson, Membrane system design for multicomponent gas mixtures via mixed-integer nonlinear programming, Comput. Chem. Eng., 24 (2000) 2719-2737. https://doi.org/10.1016/s0098-1354(00)00625-6.